Article

Enhancement of Graphene Coated Para-Aramid Yarns Pull-Out Resistance by Laser Pre-treatment

Silvija Kukle , Lyubomir Lazov , Rynno Lohmus , Ugis Briedis * , Imants Adijans , Ieva Bake , Vladimir Dunchev , Erika Teirumnieka

Posted Date: 16 March 2026

doi: 10.20944/preprints202603.1177.v1

Keywords: laser pre-processing; nano/microstructures; CW CO2 laser; Kevlar® KM2 fibers; graphene modified; surface roughness; yarn pull-out force

 doi:10.20944/preprints202603.1177.v1

Article

Enhancement of Graphene Coated Para-Aramid Yarns Pull-Out Resistance by Laser Pre-treatment

Silvija Kukle [1], Lybomir Lazov [2], Rynno Lohmus [3], Ugis Briedis [1,*] Imants Adijans [2], Ieva Bake [1], Vladimir Dunchev [4] and Erika Teirumnieka [2,]

[1] Institute of Architecture and Design, Riga Technical University, LV-1658 Riga, Latvia
[2] Rezekne Academy, Riga Technical University, LV-1658 Riga, Latvia
[3] Faculty of Science and Technology, Institute of Physics, University of Tartu, 50090 Tartu, Estonia
[4] Department Material Science and Mechanics of Materials, Technical University of Gabrovo, 5300 Gabrovo, Bulgaria
* Correspondence: Correspondence: ugis.briedis@rtu.lv; Tel.: +371-29-408-119

Abstract

This study investigates the feasibility to enhance graphene coated para-aramid yarns pull-out resistance from fabric structure, junction rupture force (JRF) increasing the fiber surface roughness with nano- and microstructures obtained by the laser irradiation and graphene coat. Two types of Kevlar® KM2 fibers woven fabrics subjected to the (CW) CO2 laser processing to investigate influence on yarn pull-out force from fabric structure upon various combinations of laser power and scanning speed using fixed laser spot diameter and raster step. Depending on the combination of applied laser parameters, a JFR increase of between 50 and 90% was achieved for laser irradiated KM2+ 440 fabric compared to the JFR of untreated fabric. By applying a single layer of graphene to the fabric with an optimal laser parameter set, JRF doubles, after the second layer is applied it triples, indicating that cumulative effects are produced. The AFM and SEM images studies of the self-organization of nano- and microstructures on the surface of Kevlar® KM2 fibers allow us to conclude that the irradiation-induced structures are forming in the defect-enriched upper nanolayer of the fiber skin, which is about 8 nm thick. Treatment within the examined laser parameter limits does not affect the fibers core structure.

Keywords: laser pre-processing; nano/microstructures**;** CW CO2 laser; Kevlar® KM2 fibers; graphene modified; surface roughness; yarn pull-out force

1. Introduction

Aramid fibers (AF) are widely used in various industries due to their exceptional strength, durability, and heat resistance, making them ideal for applications in aerospace, automotive, military, and personal equipment. Para-aramids (Kevlar®, Technora®, Twaron®) are also used for thermal protection, either alone or in blend form due to 60% strength and modulus retention at 260 °C [1]. These fibers do not melt but chars to a black color. Aramids are resistant to many solvents, have low water absorbency, but are sensitive to ultraviolet (UV). However, due to the chemical inertness, high crystallinity, and smooth surface, AF often needs surface modification to improve the chemical bonding and mechanical interlocking between the fibers and matrix [2–4]. The surface modifications of AF can improve the surface chemical activity and increase the surface roughness, which aims to achieve an external chemical boning and mechanical interlocking between fiber and matrix [5].

Various surface modifications methods employed to modify AF, such as chemical grafting by attaching side chains or branches to a polymer backbone [6], physical methods – plasma treatment [7], Y-ray and UV irradiation [8], application of different coatings [9], nanostructure construction on surfaces [10–12].

 doi:10.20944/preprints202603.1177.v1

Several laser treatments have been successfully exploited in the textile industry for decades. In laser processing widely used in textile production technologies - marking, engraving, cutting, welding, laser-based denim fading, laser ablation or additive manufacturing, obtaining the required function is associated with partial or complete destruction of material in the processing zone [3–16]. Non-destructive techniques including fabric fault detection and objective evaluation of seam pucker [13,14] along with the three-dimensional scanning application for custom-fit garments production [13] and in designing practice [17] gain wider use now. The use of laser systems for processing textile polymers increases due to speed, accuracy and flexibility [16], as well due to the emergence of new laser techniques for implementation

Laser surface texturing (LST) and laser induced periodic surface structures (LIPSS) are being intensively explored to investigate and harness the advantages of laser micro/nano processing for surface functionalization [18]. These research activities involve design of surfaces for different applications; modeling and setup of laser processing parameters; tailoring surface properties by laser irradiation; characterizing the processed surfaces using both experimental and analytical methods and testing the engineered surfaces in proposed applications [18].

LST technologies alters the surface properties of a material by modifying its texture and roughness with the high-intensity laser beams. Focused laser beam selectively remove material from the surface through localized melting, vaporization, or ablation [19], increasing the surface area and aspect ratio, thus creating large anchoring area of sensitive materials to obtain high-quality functional coatings. Experimentally was shown the adhesive bond strength is linearly proportional to the contact area [20]. Thus, LST can enhance adhesion characteristics, alter friction coefficients [21] and reduce the wear rate [22].

LST is based on self-organized laser irradiated structures and direct laser-inscribed structures. The possibilities are limitless for laser-inscribed structures, whereas for laser-irradiated structures only two main types - random and periodic structures - reported [23]. The self-organized surface structures may consist of microstructures, nanostructures, or hybrid variants [24]. So far, there are few reports on the range of applications of the laser-irradiated structures compared to the wide range of applications offered by laser-inscribed structures [25,26]. The possible technological constraints of laser processing are largely determined by the expected processing effects and the structure specifics of material subjected to processing and its diverse properties as material [27].

Suited for textile treatments are carbon dioxide (CO2) lasers providing targeted heating to a portion of the material surface creating photo thermal effect. Depending on the wavelength, the penetration depth of most materials ranges from a few microns to hundreds of microns. Heat dissipation in a sample, which is affected by its thermal conductivity and the nearby environment adjacent to the irradiated region, forms a “heat affected zone [27]. In the photothermal process, the energy received from the laser beam increases the surface temperature of the material, leading to melting and/or vaporization. Photothermal processes induce surface modifications such as roughness in polymers. However, in the photochemical process, there is a direct breakage of molecules by highly energized photons incident on a material surface, hence inducing chemical modifications. The combination of both photothermal and photochemical processes modify the roughness and chemistry of surfaces simultaneously [28].

Laser marking on the fly refers to a marking technology that allows products to be marked while moving on production line, without the need to stop the process. In this non-stop marking technology, the laser system synchronizes with the speed of the moving product [29]. Unlike traditional stationary marking, this method enables real-time engraving, coding, or serial numbering while the product passes under the laser beam (Figure 1a). This ensures no slowdown in production speed, making it ideal for high-volume manufacturing. This advanced method ensures high-speed, high-accuracy identification and processing can reach 1600 mm in width, supporting textile unwinding, modifying and rewinding.

 doi:10.20944/preprints202603.1177.v1

(a) (b)

Figure 1. Golden Laser Roll-to-roll System for continuous textile processing; (**a**) directed CO2 laser beam; (**b**) Galvano laser roll-to-roll engraving machine [30,31].

Recently launched the roll-to-roll laser treatment system (Figure 1b) equipped with advanced CO2 laser that can create continuous effects on textile roll goods in a variety of finishing techniques including cutting, engraving, perforating and marking maintaining consistent quality through the entire roll. This technology opens new possibilities for modifying para-aramid woven, knitted, and non-woven textiles surfaces with laser-irradiated micro and nanostructures.

This study investigates the feasibility of increasing graphene coated para-aramid yarns pull-out resistance from fabric structure applying its fibers surface micro/nano patterning by the laser pre-treatment. Two types of Kevlar® KM2 fibers woven fabrics subjected to the (CW) CO2 laser processing to investigate influence on yarn pull-out force from fabric structure - Junction Rupture Force (JRF) upon various combinations of laser power and scanning speed using fixed laser spot diameter and raster step whose values were determined in previous studies [24].

2. Materials, Experiment Setup and Methodology

2.1. The Laser Pre-Processing Specifics of Kevlar® Fibers and Fabrics

The failure mode of the aramid/resin composite is generally interfacial debonding with some fibrillation of the fiber surface [32,33] relevant to the skin/core structure formed in the aramid fiber extrusion and coagulation process [34], which is different from the carbon fiber reinforced composite [4]. The core region tends to possess a high degree of order and crystallinity, while the microstructure of the skin is generally less crystalline [35]. The molecular interactions in the skin region are weak so that micro fibrils can be detached from the fiber surface [33]. The special skin/core structure of the aramid fiber makes the interfacial failure mechanisms highly intricate. The quantitative effects of the skin/core structure of aramid fiber on its adhesion properties are still not fully investigated.

It was found that in contrast to the mostly chemically based interfacial property improvements achieved by oxygen plasma treatment of aramid fibers, laser ablation of aramid fibers induces surface micro-corrugations that lead to a 120% improvement of the interfacial shear strength of aramid fiber. A simple model based on an elementary analysis of the expected strain field in the presence of interface corrugation was found to provide a quantitative explanation of the observed strength enhancement factors [36]. Micrometer-sized surface corrugations produced on Kevlar® fiber surfaces by laser ablation were found to dramatically enhance the mechanical adhesion between the fibers and the epoxy matrix in a fiber-reinforced composite. Symmetric and asymmetric corrugation structures were produced by irradiating the fibers with high-fluence UV laser pulses at various incidence angles.

It is supposed in current research that laser pre-processing could increase the graphene coating adhesion to the aramid fibers as previous experiments testify the significant increase of Kevlar® fibers surface roughness and yarns pull out force from the fabric [24].

The inhomogeneity in the aramid fibers and yarns properties and fabric structures [24] make the fabric laser machining difficult, process can significantly affect these materials, leading to various

 doi:10.20944/preprints202603.1177.v1

forms of damage, such as fibers fibrillation, skin fragments pull-out and structure damage as well heat damage. Thus, laser processing of fabric involves numerous parameters, which need to be optimized to achieve the required outcomes. These parameters include applied laser power, repetition rate and scanning speed, and a wide range of material parameters [16]. The effect of these parameters on process behaviors includes heat-affected zones, machining depth and material removal rate. The one-factor variation at a time approach commonly used requires many runs and does not allow for the investigation of process variable interactions.

Power (P) and raster setup determine the energy delivered. Laser speed (LS), often referred to as scanning speed, determines the duration of laser exposure on any part's surface and indicates how quickly the laser beam moves across the material surface during the LST process. LS influences the depth, quality, and overall appearance of the produced effects as well impacts several facets of laser processing, including precision, efficiency, and material integrity. At lower speeds, the laser beam dwells longer on each point of the material, delivering more energy to the area. This increased exposure results in deeper and more intense marks, requiring significant material removal or high contrast, but may also lead to excessive heating and potential material damage. This can cause unwanted effects such as melting or charring, particularly in heat sensitive materials like polymers.

Higher LS reduces the time spent on any one point, leading to shallower and less intense marks. This is suitable for surface treated applications where only a slight alteration of the material is desired, such as light etching or marking coated surfaces. Polymers are more sensitive to heat and can benefit from higher speeds to prevent melting or evaporation. Fast LS are more likely to have minimal thermal impact and produce cleaner marks. When marking depths of 0.127 mm or deeper is required, making multiple passes with high-speed settings can be more efficient than marking at lower speed settings. However, if the LS are set too high, the laser might not generate enough heat to produce the necessary effects. When the laser beam contacts the surface of the material, its concentrated energy causes controlled vaporization in case of aramid. Depending on the settings—power, speed, and raster setup—this produces either subtle etchings or profound engravings.

Even if these three main CO2 laser parameters are coordinated to ensure the planned intensity of fiber surface modification, local heat damage may occur due to structural irregularities and defects on the fabric surface. The most common heat damage of varying intensity affects the fibers raised on the fabric surface, especially when defects resulting from technological processes have accumulated there [24].

SEM micrographs show (Figure 2) as the heat of the laser beam increases micrometer-sized surface corrugations produced on Kevlar® fiber surfaces by laser ablation (Figure 2a) that can locally increase the diameter of the affected fibers (more common defect) (Figure 2b). This indicates that under increased heat, evaporation of the aramid fiber core occurs, and volatile compounds accumulate under the skin. As the volume of accumulated volatile components increases, cracks initially appear in the skin (Figure 2c), the fiber diameter further increases until the skin completely decomposes, revealing deep internal core structural damage caused by evaporation (Figure 2d). In most cases, the damage affects two or even several adjacent fiber areas.

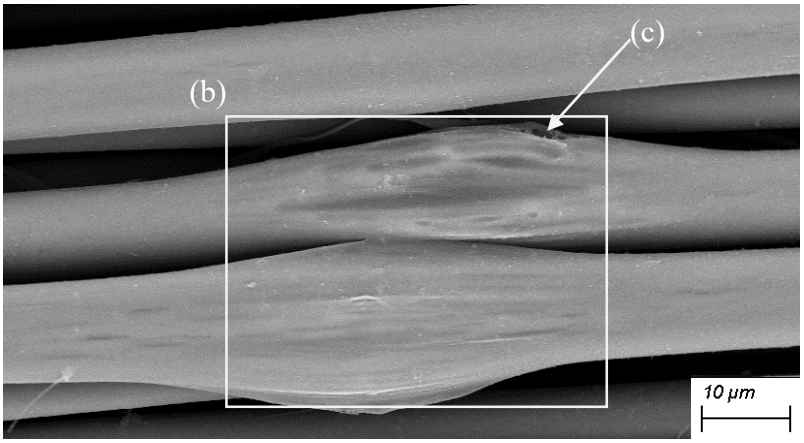

 doi:10.20944/preprints202603.1177.v1

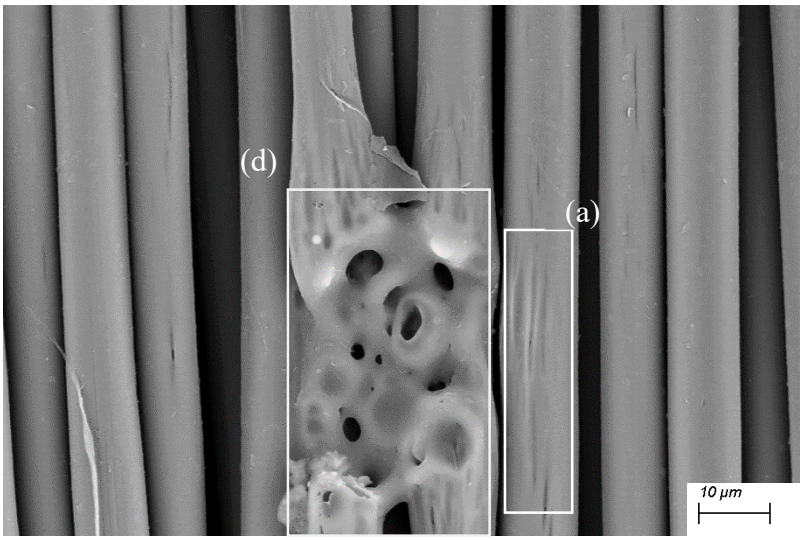

Figure 2. Local heat damage. Mag, 1.000 KX.

Thus, the destruction of the outer fibers begins beneath the fiber skin, with gaseous compounds accumulating and causing local attacks on the fiber skin. Cracks in the skin appear in directions of lower resistance, which, upon reaching a threshold, can result in the disruption of the fiber architecture, forming porous, thin-walled structures with pore sizes ranging from the nanometer level to several tens of micrometers (Figure 2d). If the laser parameters are not adjusted, the degradation process continues, leading to the complete evaporation of fragments of the overheated fiber groups [24]. Intensive or less intensive damage can be visually observed by the intensity of the color changes in the fabric. Fiber groups exposed to local damage are those that have risen above the fabric plane at yarn intersections, as well as in areas where defects have accumulated (fibrillated fibers, tufts of torn in previous processes skin fragments, clusters of applied finishes, etc.). Areas with high surface contamination combined with the local elevation of individual fibers, more often fiber groups, above the fabric plane are more susceptible to the local fiber structure damage (Figure 3a). Laser processing of less contaminated surfaces (Figure 3b) with the same set of processing parameters occurs without causing deep damage (Figure 2d) to the fiber structure**.** The author's experience indicates that after laser processing with the experimentally applied laser parameter sets, the number of defects created by previous technologies is significantly reduced.

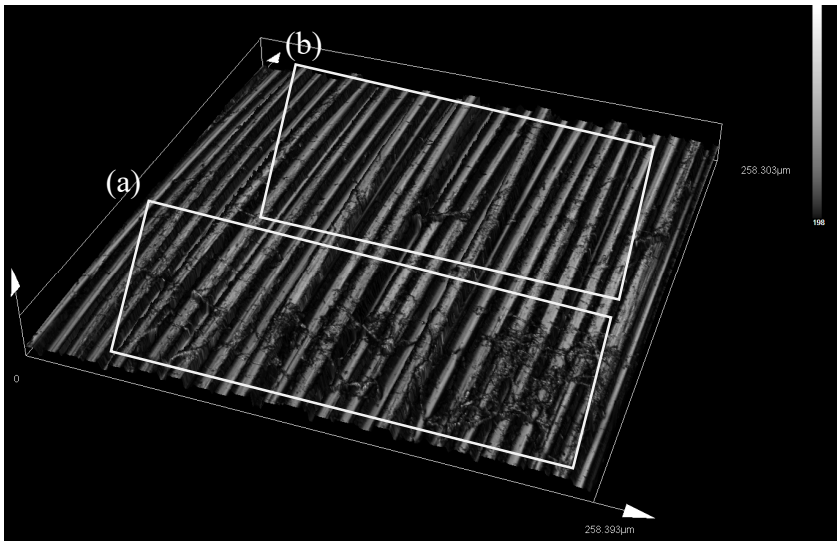

Figure 3. Confocal 3D image of as received KM2 600 fabric. Mag., x 1125.

 doi:10.20944/preprints202603.1177.v1

The damage to the outer fiber skin shown in Figure 4 is less common and occurs when the laser working head touches the fibers that have risen above the plane of the fabric.

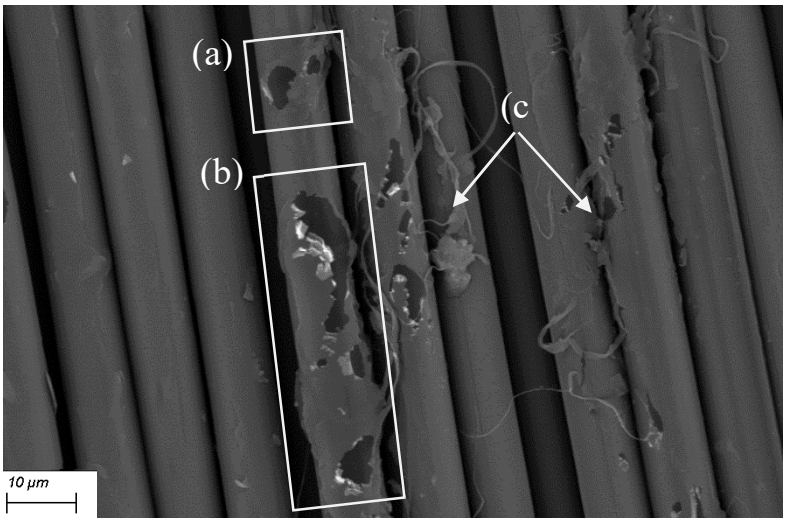

Figure 4. SEM image shoved damaged by laser working head skin of fibers that rise above the fabric plane. Mag, 1.000 *KX*.

2.2. Materials

Two types of Kevlar® KM2 fibers ballistic fabrics used: 1) KM2+ 440 (producer SAATI S.p.A, Milano, Italy) loomstate, plain weave, 14 threads per cm in warp and weft direction, fabric thickness 0.17 mm, areal density 125 g/cm2; 2) KM2 600 (INFINITY COMPOSITES INC, US), plain weave, 11 threads per cm in warp and weft direction, fabric thickness 0.23 ± 0.02 mm, areal density 146 g/cm2, final UV protection finishing. Both fabric types subjected to the laser pre-processing with the following modifying with graphene coating.

2.3. Laser Pre-Processing

Continuous Wave (CW) CO2 Laser SUNTOP Model: ST-CC9060 (Suzhou Suntop Laser Technology Co, Ltd., Suzhou City, China) producing a continuous beam of 10.6 µm wavelengths used. Beam diameter in focus d = 100 µm and focal length F = 63.5 mm were kept unchanged. As variables in this study used laser beam Scanning Speed (v), Power (P) and Raster Step (Δx), variant designation and corresponding parameter set-ups and seen in Table 1.

Table 1. Laser pre-processing parameters set of fabric samples.

Designation	Power, w	Laser speed, mm/s	Frequency, µm
V1_Laz	1.262	150	80
V2_laz	0.455	150	80
V3_laz	1.262	100	80
V4_laz	0.455	100	80
V0_laz	0.905	120	80

2.4. Technology to Obtain Graphene Coating on Laser Pre-Processed Fabric Samples

Method and technological sequence to obtain graphene-modified Kevlar® fabric developed by authors [37–39] used to produce graphene modified samples using laser pre-processed Kevlar® KM2+ 440 and Kevlar® KM2 600 woven fabrics. Samples processing plan seen in Table 2

Table 2. KM2+ 440 and KM2 600 fabric processing plan.

Designation	Laser processing	Graphene coating

 doi:10.20944/preprints202603.1177.v1

	1x	1k	2k
KM2+ 440			
V1_laz	x		
V1_1k	x	x	
V1_2k	x	x	x
V2_laz	x		
V2_1k	x	x	
V2_2k	x	x	x
V3_laz	x		
V3_1k	x	x	
V3_2k	x	x	x
V4_laz	x		
V4_1k	x	x	
V4_2k	x	x	x
V0_laz	x		
V0_1k	x	x	
V0_2k	x	x	x
KM2 600			
KM2 600_1k		x	
KM2 600_2k		x	x
V2_KM2600_laz	x		
V2_KM2600_laz_1k	x	x	
V2_KM2600_laz_2k	x	x	x
V3_KM2600_laz	x		
V3_KM2600_laz_1k	x	x	
V3_KM2600_laz_2k	x	x	x

2.5. Surface Morphology Investigation

Confocal laser scanning microscope OLYMPUS LEXT 3D MEASURING LASER MICROSCOPE OLS5000 model "OLS5100-EAF" (Olympus Corporation, Tokyo, Japan) and Atomic Force Microscope Dimension Edge (Veeco) (Institute of Physics at University of Tartu, Estonia) used to obtain surface images, graphs and roughness evaluation. SEM ZEISS (Oberkochen, Baden-Württemberg, Germany, located in the Vasil Levski National Military University, Bulgaria) used to investigate laser pre-processed and graphene modified Kevlar® fabric samples surface morphology. Sputter coatings with gold were applied to prevent nonconductive Kevlar® samples charging and enhance image quality.

2.6. Quasi-Static Yarn Pull-Out Test Methodology

Thread-pullout experiments were performed with the device Instron Force transducer model 2519-107 (capacity: 5000 N, model 2519-107, ID:3345K6537, Illinois Tool Works Inc., Norwood, MA, USA) and results were observed with the program Instron Bluehill Lite Version 2.17., SN: 717479C, Illinois Tool Works Inc., Norwood, MA, USA). Ten threads were pulled for each sample, and every fifth thread was pulled out. Two samples have been prepared for each variant in a size of 220 mm in the warp and 110 mm in the weft direction according to the methodology [24,40,41].

3. Results

Kevlar® KM2+ 440 and KM2 600 fabrics samples were prepared by performing pre-treatment using laser parameters according to the variants (Table 1). After laser pre-treatment, the fabric samples were subjected to the technology of graphene deposition as one (designation 1k) or two-layer (designation 2k) coatings following plan specified in Table 2.

 doi:10.20944/preprints202603.1177.v1

3.1. Experimental Results of Processed Kevlar® KM2+ 440 JRF Tests

Results of processed Kevlar® KM2+ 440 JRF tests obtained using quasi-static yarn pull-out test methodology seen in Table 3. Data in the first line of Table 3 refers to the unmodified reference sample. In the last column, increased percentages are shown to evaluate the relative contribution of each treatment.

Table 3. Processed KM2+ 440 fabric samples junction rupture force and tensile stress.

	Junction rupture force, N			Tensile stress, %			JRF increase compared to
	Range	Mean	-/+	%	Mean	-/+	KM2+ 440, %
KM2_440	0.38	2.42	0.04	1.20	2.37	2.15	
V1_laz	0.53	3.65	0.05	0.70	2.10	2.15	50.8%
V1_1k	1.04	5.87	0.10	0.90	2.32	2.15	142.7%
V1_2k	1.33	6.36	0.16	2.10	2.57	2.15	163.2%
V2_laz	0.80	4.82	0.08	1.20	2.74	2.15	99.4%
V2_1k	0.34	6.85	0.04	1.10	2.90	2.15	183.4%
V2_2k	2.31	10.23	0.23	0.80	3.92	2.15	323.3%
V3_laz	0.42	4.68	0.05	1.20	2.74	2.15	93.5%
V3_1k	1.56	5.60	0.15	0.80	2.79	2.15	131.5%
V3_2k	1.50	7.84	0.19	0.50	3.11	2.15	224.5%
V4_laz	0.58	4.10	0.07	0.80	2.43	0.10	69.7%
V4_1k	0.87	4.25	0.08	1.60	2.85	0.21	75.9%
V4_2k	0.62	6.64	0.09	1.60	3.35	0.17	174.6%
V0_laz	0.67	3.18	0.04	0.40	2.00	0.11	31.6%
V0_1k	1.22	5.90	0.12	0.70	2.35	0.07	144.1%
V0_2k	0.64	6.73	0.07	1.20	2.90	0.11	178.4%

As can be seen from the data in Table 3, the laser pre-treatment of the KM2+ 440 fabric surface within the applicable Power and Scanning speed limits increases the average JRF values by 50% up to 90% compared to the average JRF values of an equivalently precleaned untreated samples. Figure 5 clearly shows that the set of laser parameters corresponding to variants V2 and V3 caused the largest changes in the average JRF values, to 99% and 94%, respectively as can be ascertained in the last column of Table 3.

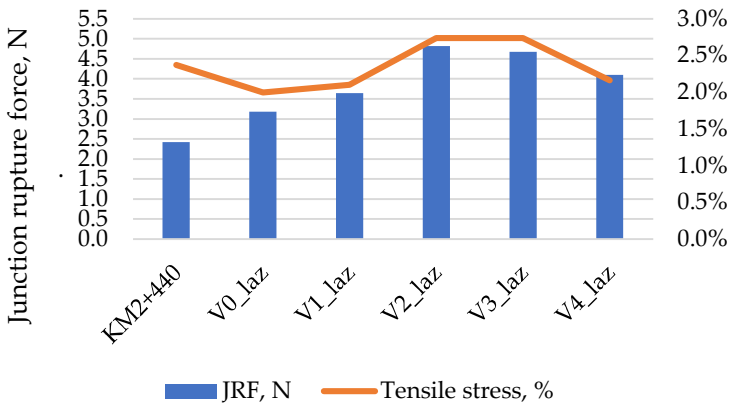

Figure 5. Junction rupture force and tensile stress changes after treatment with a (CW) CO2 laser depending on beam power and scanning speed at a frequency of 80 μm/s.

The particularly pronounced effect of laser pre-treatment is visible on the average JRF value of the V2 samples modified with following graphene coatings (Figure 6), especially if two layers

 doi:10.20944/preprints202603.1177.v1

deposited. It is not difficult to notice that the increase in the average JRF value of the graphene-modified samples follow the corresponding increased tendency in the laser pre-treatment JRF values.

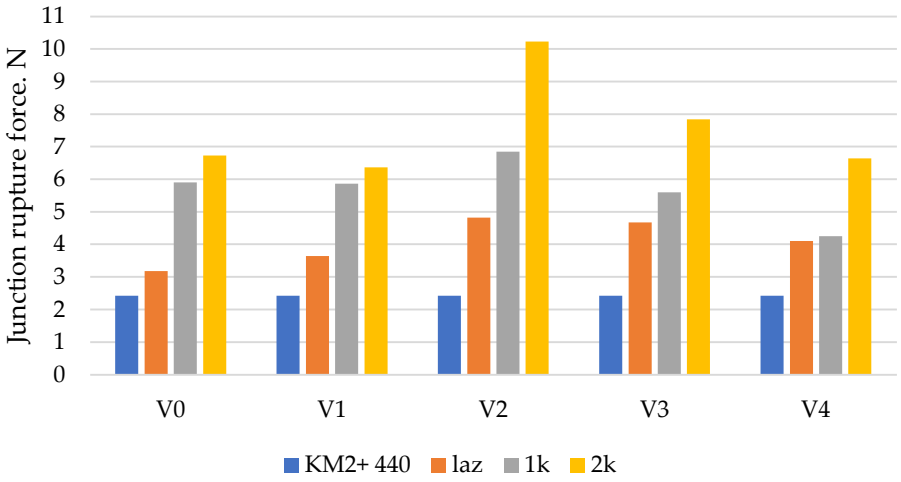

Figure 6. Effects of laser pretreatment on graphene-modified KM2+ 440 fabric samples JRF.

Response surface and corresponding contour plots (Figure 7) show highest relative JFR increase of graphene coated KM2+fibers fabric in area surrounded by a combination of lower used Power values with the higher laser beam movement speed. This trend correlates with the JRF values obtained by testing only samples subjected to laser pre-treatment (Figure 5, 6) and indicates the efficiency of laser pre-treatment by significantly increasing the yarn pull-out resistance from KM2+ fiber 440 dtex yarns woven fabric structure modified graphene coating.

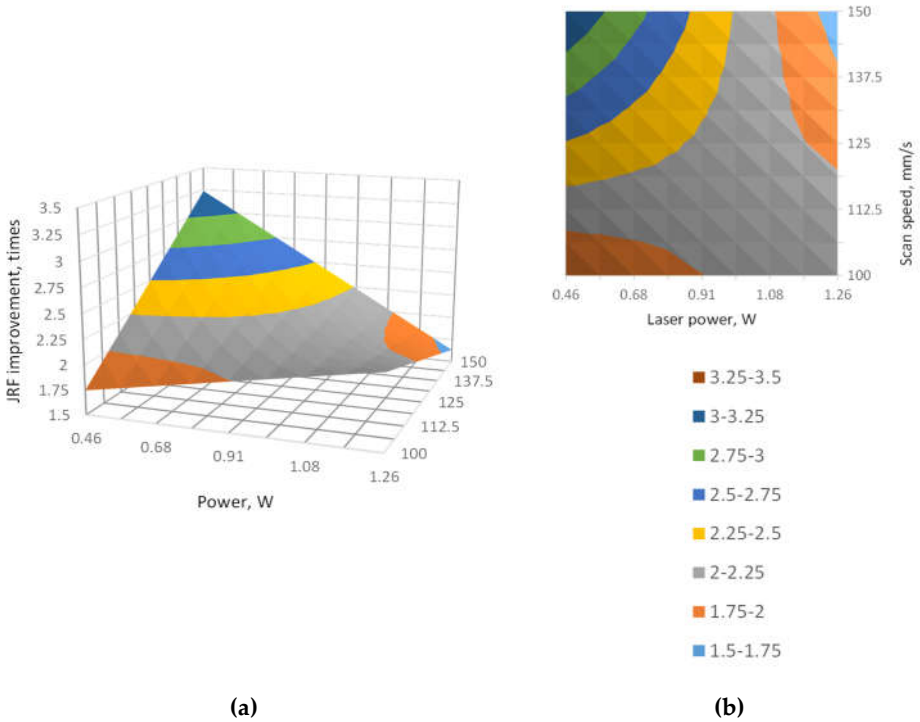

(a) **(b)**

Figure 7. Laser pre-processing parameters influence on the JRF improvement of graphene coated KM2+ 440 fabric; (**a**) response surface, (**b**) contour plots.

It is possible that the obtained yarn pull-out high resistance could be strongly influenced by the properties of the KM2+ 440 fabric structure**.** It is relatively light, tightly woven plain weave ballistic

 doi:10.20944/preprints202603.1177.v1

grade fabric (14 threads per cm in warp and weft direction, thickness 0.17 mm, areal density 125 g/cm²).

3.2. Experimental Results of Processed Kevlar® KM2 600 JRF Tests

For comparison, the effects of laser pre-treatment on KM2 600 fabric were examined (600 dtex threads, plain weave, 11.2 threads per cm in warp and weft direction, fabric thickness 0.23 mm, areal density 146 g/cm²) applying the V2 and V3 variants of laser treatment options as more effective to apply to the previously analyzed fabric.

Results of yarn pull-out tests of processed Kevlar® KM2 600 fabric samples seen in Table 4. Data in the first line of Table 4 refers to the unmodified reference sample KM2 600. In the last column, increased percentages are shown to evaluate the relative contribution of each treatment.

Table 4. Processed KM2 600 fabric samples junction rupture force and tensile stress.

Variants	Maximum Load, N		Tensile stress, %		increase compared to KM2 600
	Mean	-/+	Mean	-/+	%
KM2 600	5.49	0.33	4.37	0.36	
KM2 600_1k	6.84	0.34	3.79	0.13	24.7%
KM2 600_2k	9.48	0.24	4.25	0.20	72.8%
V2_KM2600_laz	6.79	0.06	3.59	0.18	23.7%
V2_KM2600_laz_1k	8.30	0.46	3.91	0.15	51.2%
V2_KM2600_laz_2k	10.13	0.44	4.21	0.23	84.6%
V3_KM2600_laz	5.92	0.33	3.81	0.23	7.9%
V3_KM2600_laz_1k	6.95	0.18	4.30	0.16	26.6%
V3_KM2600_laz_2k	8.14	0.18	3.58	0.17	48.4%

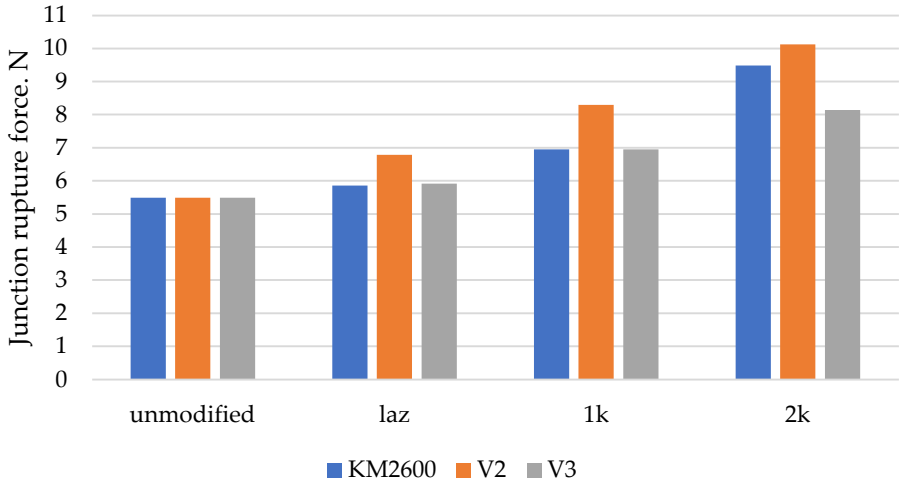

Figure 8. Effects of laser pretreatment on graphene-modified KM2 600 fabric samples JRF.

Comparing the percentage changes in JRF shown in Table 4 and the changes in average JRF values shown in the graph depending on the applied modifications, it is evident that the effect of laser pre-treatment is significantly weaker compared to KM2+ fiber fabric. These obvious differences can be partly explained by the different fabric structure parameters and the much larger number of fibers in the cross-section of the yarns. The purpose of the applied modification is not to create changes on the macro level of the fabric surface, as occurs, for example, in engraving or welding processes. During the experiment, the sets of laser processing parameters applied change the very smooth surface of Kevlar® fibers, creating nano- and/or micro-structures on them with the aim of ensuring better adhesion with coatings or matrices while maintaining the mechanical and other application-relevant properties of fibers.

 doi:10.20944/preprints202603.1177.v1

4. Discussion

4.1. Self-Organization of Laser Irradiated Nano- and Micro-Structures

Currently, several theories are being considered that provide an opportunity to describe surface structures that arise when a laser beam acts on the material's surface. When studying the effect of laser processing on polymer surfaces, the theories of light-induced material reorganization are considered more suitable. Material reorganization theories focus on reshaping laser-irradiated material into a topography characterized by a periodic combination of grooves and ridges. The mechanisms underlying this theory, which are currently under investigation, include thermodynamic phase transitions, hydrodynamic effects of the transiently melted surface, and unstable phases of the material during irradiation, accumulation of defects, diffusion, and surface erosion. Molecular Dynamics (MD) modeling applied for these effects studies predicts the kinetic trajectory of an ensemble of atoms as the laser interacts with the solid. This is achieved by numerically solving Newton's equations of motion spatial-temporally at the atomic scale [42].

Solutions rely on local surface gradients, which require the surface to remain in an unstable, metastable state for a sufficient time interval to induce material reorganization. Usually three laser-irradiation regimes are considered to differ by the laser fluences needed for the nano- and micro-structuring (NMS) of surfaces. In the regime of a relatively low subthreshold fluence, the NMS formation results from multi-pulse irradiation in the absence of the melting of a solid [43]. The most salient feature for all types and regimes of irradiation is the universal behavior of the lateral size of the structure, which can be interpreted as a linear dependence of the lateral size of the nano- and micro-structures on the thickness of the defect-enriched layer formed due to the energy deposition. This experimental dependence is revealed for all irradiation types and regimes. The irradiation results in the formation of a nanometer thick subsurface defect-enriched stressed layer h. The nature of this nanolayer, thickness and the stress in it, and the defect types depend on the material properties, irradiation regime and type, and must be determined in each case.

Defects in layer h have enhanced the lateral mobility due to the nonequilibrium conditions for the defect generation (charging of point defects, heating, a relatively high level of plasma excitation, ion-stimulated and stress-enhanced diffusion, etc.). Thickness h of the defect-enriched nanolayer serves as the first scaling parameter that determines the NMS lateral dimensions [44].

Defect rich layer of laser processed KM2+ 440 fabric variant V0_laz does not exceed 23 nm (Figure 9a). This means that surface roughness changes obtained in result of the laser treatment located in the fiber skin and does not affect its core structure. The KM2 fiber skin thickness is estimated to be in the range of 300-350 nm [45,46]. Point defects in layer h form individually, but most often in smaller or larger groups as show blue arrows (Figure 9b) and around them, nanoscale bumps and cavities are formed (Figure 9a and b). Lateral size R of defects measured from AFM micrographs range from a few tens to a few hundred nanometers (Figure 9c and d) and Figure 10). The average thickness of the defect-enriched nanolayer KM2+ fibers are estimated at h ~ 8 nm (Figure 9d and e). It means that it is upper layer of KM2+ fiber skin which thickness is less than a micrometer.

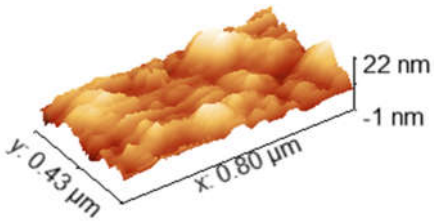

(a)

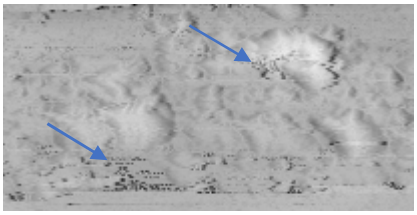

(b)

 doi:10.20944/preprints202603.1177.v1

V0_laz	R, nm	Δz, nm
1	193	-1.61
2	79	-1.41
3	90	-3.92
4	55	1.55

(d)

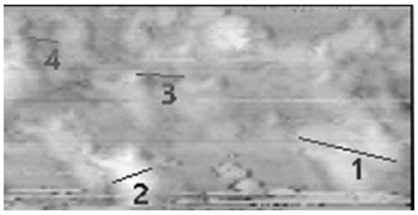

(c)

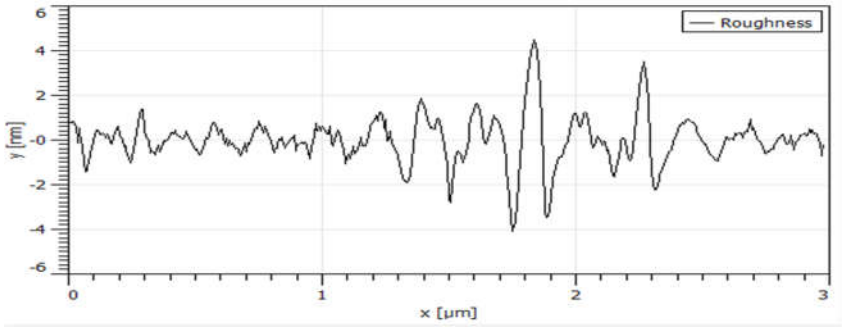

(e)

Figure 9. AFM micrographs of Kevlar® KM2+ 440 fabric variant V0_laz and effects of surface laser processing.

The average surface roughness Sq = 5.8 nm and the corresponding surface area increase of 4.8% after laser treatment have ensured a 31% increase in the average JRF of the V0_laz variant (Table 3). The surface is mainly covered with shallow cavities whose lateral size varies from a few tens of nm to a few hundred (Figure 10).

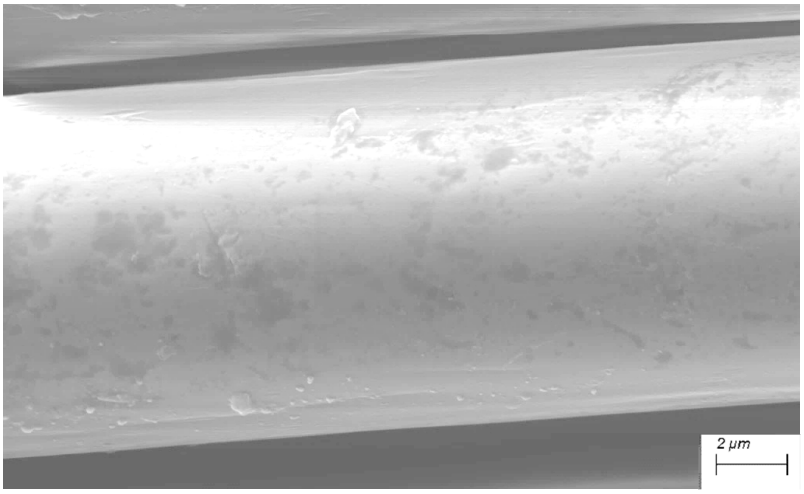

Figure 10. SEM micrograph of V0_KM2+_440_laz. Mag 5.00 K X.

Grooves ranging from 4 to several hundred micrometers in length are located on the fiber surface of the V2_KM2+_440_laz processed fiber along the axis direction (Figure 11a, b), their width varying from a few tens to several hundred micrometers, accompanied by nanoscale bumps (Figure 11c), providing a surface roughness of Sq = 6.7 nm and an increase in surface area by 14.7%.

 doi:10.20944/preprints202603.1177.v1

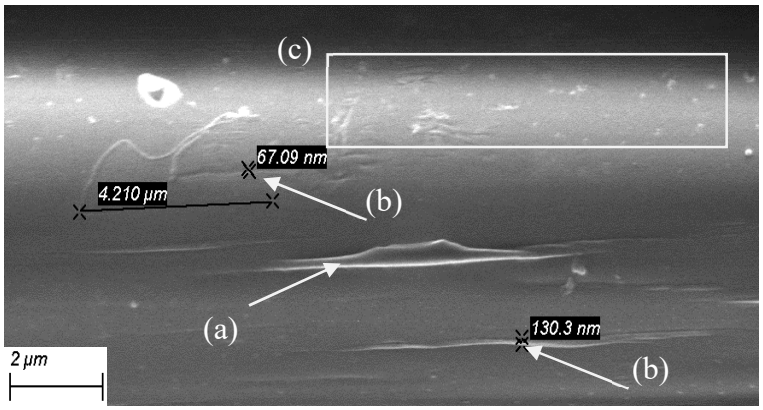

Figure 11. SEM image of laser pre-processed V2_KM2+_440_laz fiber surface Mag 6.00 K X.

With these light fiber skin surface modifications, the JRF increases at 99% (Table 3) is very significant, possibly because micro-sized grooves are combined with nano-sized bumps.

The motion of defects from the surface nanolayer along the normal to the surface (diffusion or strain-induced drift) leads to a delayed formation of the second defect enriched layer with thickness H > h. Thickness H of this expanded defect-enriched layer represents the second scaling parameter. This parameter determines the lateral large-scale modulation of the surface relief that emerges at a relatively long irradiation and that is imposed on the nanometer-scale relief. In the case of the generation of micrometer scale surface structures, parameter H determines the period of the structures [44]. Initially, the mobile point defects are uniformly distributed along the surface. A fluctuating local increase in the surface-defect concentration gives rise to the corrugation of the surface relief and the corresponding surface strain. The defects interact with this long-range surface strain field owing to the deformation potential. The strain leads to the lateral defect flux that is proportional to defect concentration and is oppositely directed with respect to the diffusion flux. At a relatively low defect concentration, the diffusion flux exceeds the strain-induced flux, the fluctuations of the spatial defect distribution decay, and the surface remains almost flat (Figure 12).

Figure 12. SEM image of V0_KM2_600_laz. Mag 3.00 K X.

The second stage of the surface structuring starts when the concentration of the mobile defects exceeds a certain critical level. At this critical point, the lateral strain-induced defect flux starts to exceed the lateral diffusion flux. From the viewpoint of the universal defect–deformation (DD) mechanism for the creation of the structures leads to the instability in which defects are autolocalized in periodic self-consistent strain wells (Figure 13c, d). Thus, the homogeneous lateral distribution of the defects is transformed into a spatially periodic (along the surface) distribution. This transformation is accompanied by the periodic corrugation of the surface with the defect piling up at the extrema of the surface relief, a ridged surface structure is formed (Figure 13a, b). Grooves typically occur in areas of the surface where a significant amount of material has been removed. The preferential orientation of grooves is generally parallel to the polarization direction of laser radiation, although in rare cases, grooves can be oriented orthogonal to the polarization [47].

 doi:10.20944/preprints202603.1177.v1

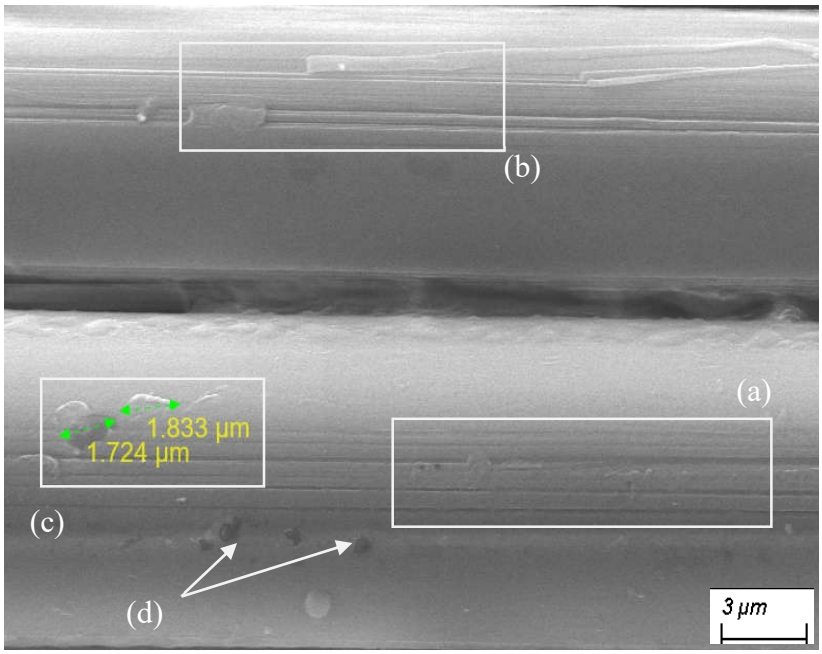

Figure 13. SEM image of laser processed V0_KM2_600_laz fibers surface. Magn. 3.00 K X.

By modifying the V2 variant Kevlar® KM2 600 fiber fabric with laser pre-treatment and applying two layers of graphene coating, its JRF has increased compared to the as-received fabric for surface fibers, respectively by 23% after laser treatment, 51% after applying the first layer of graphene, and 84% after applying the second layer (Table 4, Figure 8).

The average surface roughness Sq = 54 nm of the sample modified with a double graphene layer coating is significantly increased by multilayer graphene sheets (Figure 14a, b) with lateral sizes in the range of 200 to 300 nm.

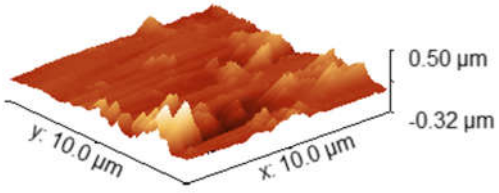

(a)

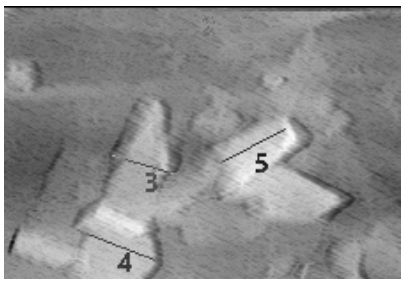

(b)

V2_laz_2k

	Sq	54.4nm
	Sa	35.2nm
	R, nm	Δz, nm
3	208	7.4
4	276	15.7
5	239	26.7

(c)

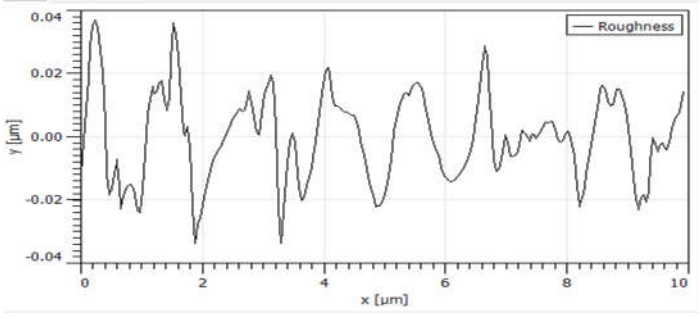

(d)

 doi:10.20944/preprints202603.1177.v1

Figure 14. AFM micrographs of Kevlar® KM2 600 fibers of variant V2_laz_2k fabric and effects of surface laser processing.

Figure 15 provides a brief insight into the interaction of laser processing with the single-layer surface modification using graphene. Graphene flakes of different lateral sizes are randomly distributed on the unmodified by laser beam surface areas without covering the laser-irradiate structures. This suggests that both effects are cumulative, indirectly confirmed by the nearly twofold increase in JRF after applying the first layer of graphene (Table 4).

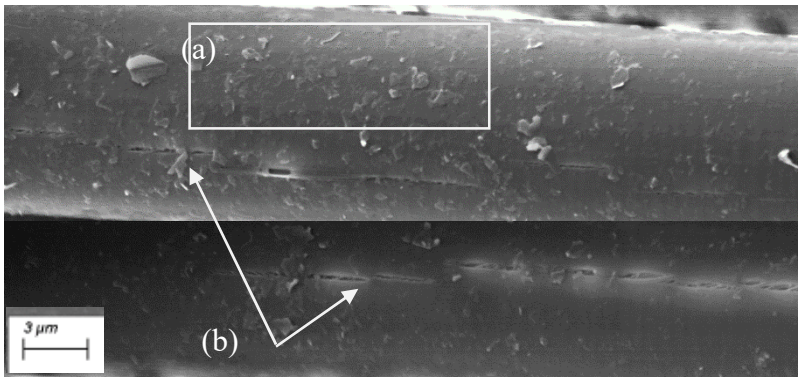

Figure 15. SEM image of laser pre-treated modified with one layer of graphene coat V3_KM2_600_1k. Magn. 3.00.K X.

4.2. Effects of Laser-Beam Defocus

An unstable focus or beam waist position on uneven surface (Figure 16) result in fluctuating laser energy density in the irradiated area, subsequently areas with varying intensity of produced topographic effects on fiber surface are formed (Figure 15) that can compromise the precision and quality of the processed surface. However, maintaining the stability of the focus beam position in laser processing is not something that is easy in micromachining and surface processing [48]. Moreover, the CO2 laser power suitable for experiments, 0.46 – 1.26, is low for fabric pre-treatment in industrial production.

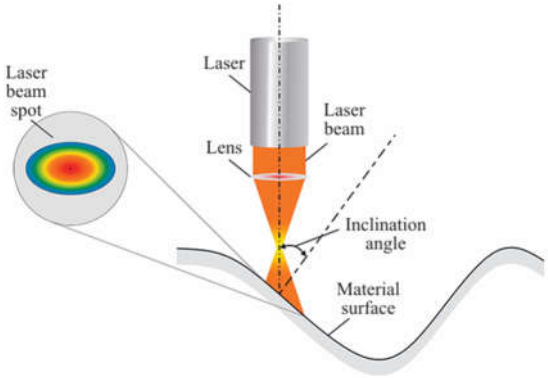

Figure 16. Uneven material surface and inclined beam — defocus laser beam spot with eclipse shape and low laser energy intensity [48].

Defocused laser beams have been used in laser cutting and welding for several decades [49–51] setting the focal plane below the surface can lead to deeper welding beads, thus increasing the productivity in keyhole welding. Two types of defocus are observed in laser processing: positive and negative defocus. Positive defocus occurs when the laser beam focuses above the material surface, aligning with the position of the focus beam. Conversely, negative defocus transpires when the focus is below the work piece or material surface, or the focus beam is positioned beneath it.

 doi:10.20944/preprints202603.1177.v1

In study [52], aimed to investigate laser beam focus shift (defocus) to increase the laser spot size in selective laser melting (SLM) of 316L stainless steel powder found that within a single laser setup, implementing defocus can lead to a potential process productivity substantial increase. Comparing positive and negative defocus distances, the negative defocus leads to a deeper melt pool due to its convergent nature. The positive defocus is less energy efficient, but also less sensitive to heat input variations, resulting in a more stable SLM process [52]. Studies of laser powder bed fusion (LPBF) indicate that modulation of the defocus distance to adjust the beam spot size is critically important and technically feasible for achieving high-quality LPBF components [53].

Based on laser beam focus shift studies in metal technologies and additive manufacturing, the authors hypothesized that the crystalline structure of para-aramids could respond similarly: In the case of positive laser beam defocus values, shallow surface structure changes (conductive node) are formed, whereas if a negative beam defocus is applied, in addition to changes in the skin layer, deeper fiber core structures are affected (keyhole mode) [50]. Regarding fiber polymers, such studies have not been found in literature reviews to date and considering the very uneven surface topography of woven textiles, they can be resource intensive. However, extensive research is needed to successfully modify the smooth para-aramid fiber surface according to the intended use, including in composite technologies using the "laser marking on the fly" principle, which is already implemented in the CO2 roll-to-roll industrial textile texturing system (Figure 1).

4.3. Some Effects of Laser-Beam Defocus Experimental Application

Considering that by changing the laser beam diameter it is possible not only to increase the process productivity, but also to control the roughness of the processed surface by applying positive defocus (Figure 17a) and higher range of laser power 19-33 W (Figure 17b) six KM2 600 fabric samples 4x4 cm variants processed (Figure 17c).

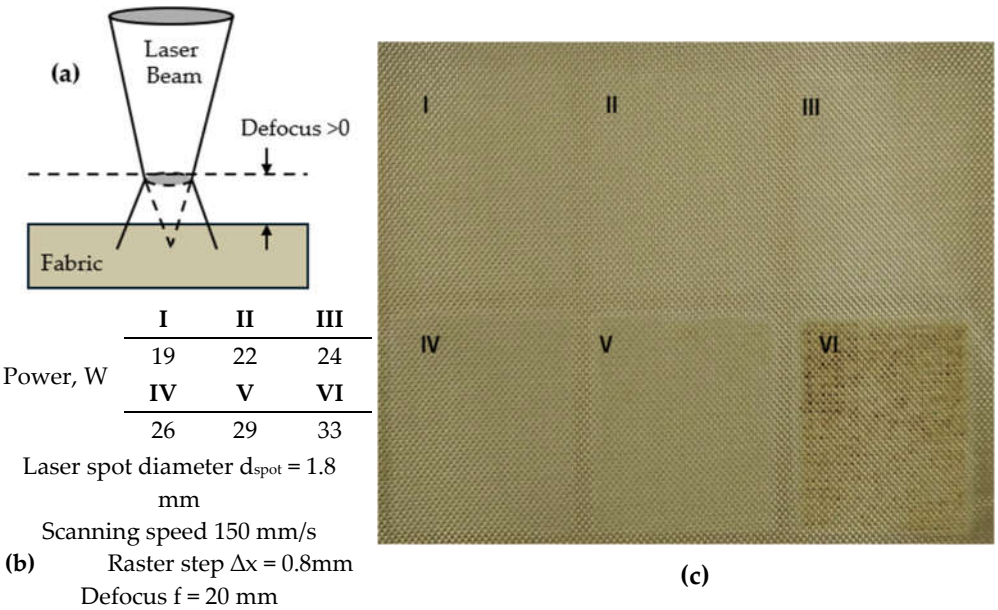

	I	II	III
Power, W	19	22	24
	IV	**V**	**VI**
	26	29	33

Laser spot diameter d_{spot} = 1.8 mm
Scanning speed 150 mm/s
(b) Raster step Δx = 0.8mm
Defocus f = 20 mm

(c)

Figure 17. Kevlar® KM2 600 fabric samples irradiated by laser defocused beam changing the power within the range of 19 to 33 W.

Max laser power 100 W. Beam diameter in focus d = 100 μm and focal length F = 63.5 mm and defocus value f = 20 mm were kept unchanged. Distance from the surface of the specimen up to the focal plane is generally defined as the defocus value. Figure 17a shows the experimental setup, where the defocus distance is positive as the focal plane is above the specimen surface. It can also be negative when the focal plane is below the specimen surface [54].

 doi:10.20944/preprints202603.1177.v1

Progressive degradation of the upper fiber layer was observed in samples of variants IV-VI (corresponding P values in a range from 26 to 33 W), therefore, for further detailed analysis, samples modified within a power range of 19 to 24 W were subjected.

The surface of pre-cleaned with acetone unmodified Kevlar® KM2 600 fabric is covered with unevenly distributed defects—mostly fibrils and torn coating fragments (Figure 18a, b). Confocal micrographs of fabric variant III laser irradiate with parameters set in Figure 17b show clean fibers surfaces without local defects caused by overheating (Figure 18a, b). Laser irradiate nano/microstructures on fibers surfaces are difficult to see due to the insufficient magnification.

To ensure a nano/micro surface texturing outcome that corresponds to the properties of the textile being processed, the fibers surface structure, and the intended use, a thorough investigation must be carried out to coordinate the set of laser parameters with the defocus value.

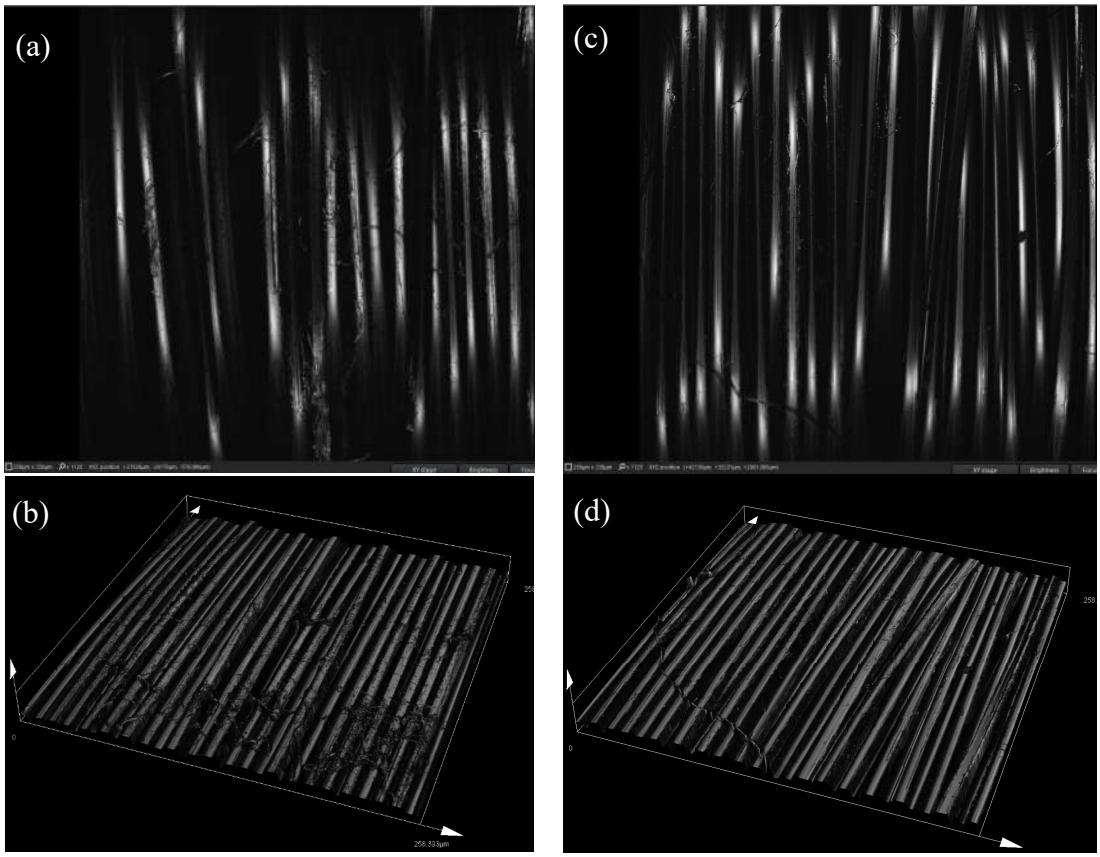

Figure 18. Confocal micrographs of unprocessed (a, b) and laser irradiated (c, d) KM2 600 fabric variant III samples. Mag., x 1125.

5. Conclusions

In this work two types of Kevlar® KM2 fiber fabrics subjected to the CO2 laser processing to investigate influence on yarn pull-out force from fabric structure JRF upon various combinations of laser power P and scanning speed v for a given raster step Δx = 80 μm and laser spot diameter 100 μm. Observations and quantitatively determined increases in JRF indicate that small changes in fiber surface roughness induced by laser irradiation of fabric surface can significantly increase JRF.

Laser processing with a specific set of parameters produces varying intensity effects depending on the characteristics of the Kevlar® fibers and fabric structure, which can be evaluated experimentally. Observations in this study suggest that a relatively smaller number of fibers per yarn and a larger number of yarns in the warp and weft directions of fabric can significantly increase JRF.

Laser nano- and microscale fibers surface modification and following functionalization with graphene coating produce cumulative effects, indirectly confirmed by the nearly twofold increase in JRF compared to unprocessed KM2+ 440 fabric.

 doi:10.20944/preprints202603.1177.v1

When studying the effect of laser processing on polymer surfaces, the theories of light-induced material reorganization are considered more suitable and this in relation to laser-irradiated KM2 fibers is confirmed by preliminary research. The set of laser parameters should be such that the thickness of the defect-enriched nanolayer is comparable to the Kevlar®® fiber skin, whose thickness for KM2 fibers is in the range of 300-350 nm and the resulting surface effects leave the fiber core structure intact.

Even if three main CO2 laser parameters are coordinated to ensure the planned intensity of fiber surface modification, local heat damages may occur due to the structural irregularities and defects on the Kevlar® fabric surface.

To improve productivity without overheating Kevlar® fibers laser spot size can be increased by shifting the focal plane and thus using a defocused beam, but serious research needs to be conducted to coordinate the laser and fabric parameters to manage the nano- and microscale fibers surface modification process on commercial roll-to-roll laser processing equipment.

During defocused nano- and microscale fibers surface modification the fabric surface is cleaned of surface-contaminating defects, including fibrils and broken skin fragments, which is important if subsequent formation of functional coatings or composites is intended.

Author Contributions: Conceptualization, S.K., L.L., R.L. and U.B.; Methodology, S.K. and L.L.; Software, R.L., I.A., I.B. and V.D.; Validation, S.K., R.L., I.A. and I.B.; Formal analysis, L.L. and R.L.; Investigation, I.A.; Resources, U.B., I.B. and V.D.; Data curation, S.K., L.L., U.B., I.A., I.B. and V.D.; Writing—original draft, S.K., R.L. and I.B.; Writing—review & editing, U.B.; Visualization, I.B.; Supervision, S.K.; Project administration, S.K. and E.T.; Funding acquisition, E.T. All authors have read and agreed to the published version of the manuscript.

Funding: This research was funded by Project Nr. 5.2.1.1.i.0/2/24/I/CFLA/003 2, Grant Technology development for obtaining functional laser nanostructured graphene coatings on para-aramid textiles to improve ballistic performance Nr.: RTU-PA-2024/1-0041. This work was supported by the Estonian Research Council grant PRG1198 and TemTa80.

Data Availability Statement: The original contributions presented in this study are included in the article. Further inquiries can be directed to the corresponding author.

Conflicts of Interest: The authors declare no conflicts of interest.

References

1. Ultimate Guide to Aramid Fibers: Types, properties and Uses – Textile engineering. Available online: https://textileengineering.net/ultimate-guide-to-aramid-fibers-types-properties-and-uses/.
2. G. Yang, M. Park, S.-J. Park. *Recent progresses of fabrication and characterization of fibers-reinforced composites: A review*. Compos. Commun. **2019**, pp. 34–42.
3. W. Lertwassana, T. Parnklang, P. Mora, C. Jubsilp, S. Rimdusit. *High performance aramid pulp/carbon fiber-reinforced polybenzoxazine composites as friction materials*. Compos. Part B: Eng. **2019**.
4. G. Qi, B. Zhang, S. Du, Y. Yu. *Estimation of aramid fiber/epoxy interfacial properties by fiber bundle tests and multiscale modeling considering the fiber skin/core structure*. Compos. Struct. **2017**, pp. 1–10.
5. Bo Zhang, Lihua Jia, Ming Tian, Nanying Ning, Liqun Zhang, Wencai Wang. *Surface and interface modification of aramid fiber and its reinforcement for polymer composites: A review*. European Polymer Journal 147; **2021**.
6. L. Loureiro, V. Carvalho, S. Bettini. *Reuse of p-aramid from industrial waste as reinforcement fiber in polyamide 6.6*. Polym. Test. **2016**, pp. 124–130.
7. Li, K. Han, H. Rong, X. Li, M. Yu. *Surface modification of aramid fibers* via *ammonia-plasma treatment*. Appl. Polym. Sci. **2014**.
8. L. Wang, Y. Shi, S. Chen, W. Wang, M. Tian, N. Ning, L. Zhang. *Highly efficient mussel-like inspired modification of aramid fibers by UV-accelerated catechol/ polyamine deposition followed chemical grafting for high-performance polymer composites*. Chem. Eng. J. **2017**, pp. 583–59.

 doi:10.20944/preprints202603.1177.v1

9. J. Chen, Y. Zhu, Q. Ni, Y. Fu, X. Fu. *Surface modification and characterization of aramid fibers with hybrid coating*. Appl. Surf. Sci. **2014**, pp. 103–108.
10. P.M. Gore, et al. *Functionalized aramid fibers and composites for protective applications: A review*. Ind. Eng. Chem. Res. **2018**, pp. 16537–16563.
11. A. Vedrtnam, S.P. Sharma. *Study on the performance of different nano-species used for surface modification of carbon fiber for interface strengthening*. Compos. Part A: Appl. Sci. Manuf. **2019**.
12. L. Zhang, H. Kong, M. Qiao, X. Ding, M. Yu. *Supercritical CO2-induced nondestructive coordination between ZnO nanoparticles and aramid fiber with highly improved interfacial-adhesion properties and UV resistance*. Appl. Surf. Sci. **2020**.
13. Nayak R and Padhye R. *The use of laser in garment manufacturing: an overview*. Fash Text **2016**; 3(5): pp. 1–16.
14. Marchant AL. *Experimental and theoretical studies of surface and volume changes in dielectrics induced by long pulse RFCO2 laser irradiation*. PhD thesis, University of Hull, UK, ***2012.***
15. Vilumsone-Nemes I. *Automated laser cutting of textile materials. In: Industrial cutting of textile materials*. 2nd ed. Woodhead Publishing, **2018**, pp. 151–177.
16. Angelova Y P. *Factors influencing the laser treatment of textile materials: An overview*. Journal of Engineered Fibers and Fabrics. **2020**; Volume 15: pp. 1 –16.
17. Rajkishore Nayak R., Padhye R. *Garment Manufacturing Technology*. **2015**, e-book.
18. F.D. Ince and T. Ozel. *Laser surface texturing of materials for surface functionalization: A holistic review*. Surface & Coatings Technology 498, **2025**.
19. Kalinowski, A.; Radek, N.; Orman, Ł.; Pietraszek, J.; Szczepaniak, M.; Bronček, J. *Laser Surface Texturing: Characteristics and Applications*. Syst. Saf. Hum.-Tech. Facil.-Environ. **2023**, 5, pp. 240–248.
20. Robin Kromer, Sophie Costil, Jonathan Cormier, Laurent Berthe, Patrice Peyre, and Damien Courapied. *Laser Patterning Pretreatment before Thermal Spraying: A Technique to Adapt and Control the Surface Topography to Thermomechanical Loading and Materials*. Journal of Thermal Spray Technology, Volume 25(3) February **2016**.
21. Stratakis E et al. *Laser engineering of biomimetic surfaces*. Elsevier Ltd. AR: Reports Mater. Sci. Eng. 141. https://doi. org/10.1016/j.mser.**2020**.
22. Gamaly EG. *The physics of ultra-short laser interaction with solids at non-relativistic intensities*. **2011**. Phys Rep 508 (4–5): pp. 91– 243.
23. Pacella M. *Pulsed laser ablation (PLA) of ultra-hard structures: generation of damage-tolerant freeform surfaces for advanced machining applications*, **2014**.
24. Kukle, S.; Lazov, L.; Lohmus, R.; Briedis, U.; Adijans, I.; Bake, I.; Dunchev, V.; Teirumnieka, E. *The Impact of CO_2 Laser Treatment on Kevlar®® KM2+ Fibres Fabric Surface Morphology and Yarn Pull-Out Resistance*. *Polymers* **2025**, *17*, 2931. https://doi.org/10.3390/polym17212931.
25. Stepak B, Antończak AJ, Bartkowiak-Jowsa M, Filipiak J, Pezowicz C, Abramski KM (**2014**) *Fabrication of a polymer-based biodegrad able stent using a CO2 laser*. Arch Civ Mech Eng 14(2):317–326. https://doi.org/10.1016/j.acme.2013.08.005.
26. Mishra S, Yadava V. *Laser beam micromachining (LBMM) - a review*. **2015**. Elsevier Ltd. Opt Lasers Eng 73:89 122. https://doi.org/10.1016/j.optlaseng.2015.03.017
27. Jelani, M., Bashir, S., Rehman, M.Ku. et al. Effect of laser fluence on surface, structural and mechanical properties of Zr after irradiation in the ambient environment of oxygen. *Eur. Phys. J. D* 67, 159 (**2013**). https://doi.org/10.1140/epjd/e2013-30767-4 .
28. Riveiro A, Maçon ALB, del Val J, Comesaña R, Pou J. *Laser surface texturing of polymers for biomedical applications*. **2018**. Frontiers Media S.A. Front Phys 5. https:// doi. org/ 10. 3389/fphy.2018.00016.
29. Hemmerich, M.; Darvish, M.; Conroy, J.; Knollmeyer, L.; Way, J. *Galvanometer scanning technology and 9.3 µm CO2 lasers for on-the-fly converting applications*. In Proceedings of the Lasers in Manufacturing **2017**, Munich, Germany, 26–29 June 2017.
30. Roll to Roll Galvo Laser Engraving machine (ZJJF(3D) – 160 0LD. Available Online: https://goldenlaser.com/roll-to-roll-galvo-laser-engraving-machine/ .
31. Laser Finishing for Textile: A Revolutionary Approach to Fabric Design. Available online: https://goldenlaser.com/blog/laser-finishing-for-textile/

 doi:10.20944/preprints202603.1177.v1

32. Andres Leal A, Deitzel JM, McKnight SH, Gillespie Jr JW. *Interfacial behavior of high-performance organic fibers*. Polymer. **2009**; 50:1228–35.
33. Xing L, Liu L, Huang Y, Jiang D, Jiang B, He J. *Enhanced interfacial properties of domestic aramid fiber-12* via *high energy gamma ray irradiation.* Compos Part B Eng **2015**;69:50–7.
34. Chatzi EG, Koenig JL. *Morphology and structure of Kevlar®® fibers: a review*. Polym Plast Technol Eng **1987**; 26:229–70
35. Roth S, Burghammer M, Janotta A, Riekel C. *Rotational disorder in poly(pphenylene terephthalamide) fibers by X-ray diffraction with a 100 nm beam*. Macromolecules **2003**;36:1585–93.
36. Bedoui F, Murthy NS, Zimmermann FM., Frank M. *Enhancement of fiber–matrix adhesion by laser ablation-induced surface microcorrugation*. **2008**. Journal of Materials Science, 43. 5585-5590 doi:10.1007/s10853-008-2805-9
37. Kukle, S.; Bake, I.; Rampane, L. *Graphene-Containing Para Aramid Fabric Coating* Via *Surfactant Assisted Exfoliation of Graphite*. Materials Today. Proceedings **2024**, 97, pp. 44–51.
38. Rampane, L.; Bake, I.; Vilc¯ena, L.; Kukle, S. *Development of Graphene-Based Functional Coating for the Surface Modification of Textiles*. Mater. Sci. Forum **2023**, 1104, pp. 77–85.
39. Kukle, S.; Valisevskis, A.; Briedis, U.; Balgale, I.; Bake, I. *Hybrid Soft Ballistic Panel Packages with Integrated Graphene-Modified Para-Aramid Fabric Layers in Combinations with the Different Ballistic Kevlar®® Textiles*. Polymers **2024**, *16*, 2106. https://doi.org/10.3390/polym16152106
40. Das, S.; Jagan, S.; Shaw, A.; Pal, A. *Determination of inter-yarn friction and its effect on ballistic response of para-aramid woven fabric under low velocity impact*. *Compos. Struct.* **2015**, *120*, 129–140.
41. Roark, J.; Thomas, F.D.; Sockalingam, S.; Kempf, J.; Christy, D.; Haas, D.; O'brien, D.J.; Senecal, K.J.; Crittenden, S.R. *Experimental Investigation of the Influence of Metallic Coatings on Yarn Pull-Out Behavior in Kevlar®®® Fabrics*. *Fibers* **2023**, *11*, 7
42. J.F. Young, J.S. Preston, H.M. Van Driel, J.E. Sipe. *Laser-induced periodic surface structure. II. Experiments on Ge, Si, Al, and brass*, Physical Review B 27 (2) (**1983** Jan 15) 1155, https://doi.org/10.1103/PhysRevB.27.1155.o.
43. S. V. Vintsents, V. B. Zaitsev, A. V. Zoteev et.al. *Low-threshold defect formation and modification of Ge surface layer under elastic and elastoplastic pulsed laser effects*. Semiconductor Structures, Interfaces, and Surfaces, **2002**. Volume 36, pp. 883–888
44. Emelyanov V.I. *Self-organization of ordered nano-and microstructures on the semiconductor surface under the action of laser radiation*, Laser Phys. 18 (**2008** Jun) 682–718, https://doi.org/10.1134/S1054660X08060029].
45. Chabi S, Dmitriy A. Dikin D A, Yin J, Percec S & Fei Ren F. *Structure-Mechanical Property Relations of Skin-Core Regions of Poly(p-phenylene terephthalamide) Single Fiber*. Scientific REPORTS. **2019**. 9:740.
46. Q.P. McAllister et al. *Evaluation of the three-dimensional properties of Kevlar®® across length scales*. J. Mater. Res., **2012**
47. F.D. Ince and T. Ozel. *Laser surface texturing of materials for surface functionalization: A holistic review*. Surface & Coatings Technology 498, **2025**. 131818
48. Rizki M.A., Fedosov Yu.V. *Analysis of the influence of defocused laser beam on uneven material surface processing based on mathematical model and simulation approach*. Scientific and Technical Journal of Information Technologies, Mechanics and Optics, **2025**, vol. 25, no. 2, doi: 10.17586/2226-1494-2025-25-2-212-22.
49. W. Schulz, G. Simon, H.M. Urbassek, I. Decker. *On laser fusion cutting of metals*. J. Phys. D: Appl. Phys. 20, **1987**, pp. 481–488.
50. D. Schuöcker. *High Power Lasers in Production Engineering*. Imperial College Press and World Scientific Publishing Company Co Pte Ltd, Singapore, **1999**.
51. J.W. Kim, B.S. Jang, Y.T. Kim, K.S. Chun. *A study on an efficient prediction of welding deformation for T-joint laser welding of sandwich panel, Part I: Proposal of a heat source model*. Int. J. Naval Archit. Ocean Eng. 5 , **2013**, pp. 348–363.
52. Metelkova J., Kinds Y, Kempen K., Formanoir C., Ann Witvrouw A., Van Hooreweder B. *On the influence of laser defocusing in Selective Laser Melting of 316L*. Additive Manufacturing 23, **2018**, pp. 161–169
53. Chang Huang, Zong-an Luo *, Hong-yu Zhou, Jin-song Yang Ming-rong Fan, Jia-xing Fu, Xin Zhan. *Effect of laser defocus on microstructural and mechanical properties of 316L stainless steel manufactured by laser powder bed fusion*. Journal of Materials Research and Technology 38, **2025**, pp. 3114–3130

 doi:10.20944/preprints202603.1177.v1

54. J.S. Kim, T. Watanabe, Y. Yoshida. *Effect of the beam-defocusing characteristics on porosity formation in laser welding*. J. Mater. Sci. Lett. 14, **1995**, pp. 1624–1626.